Peer-reviewed version available at Sensors 2019, 19, 2699; doi:10.3390/s19122699

Article

The Fiber-Optic Rotational Seismograph – Laboratory Tests and Field Application

Leszek R. Jaroszewicz [1*], Anna Kurzych [1], Zbigniew Krajewski [1], Michał Dudek [1], Jerzy K. Kowalski [2], Krzysztof P. Teisseyre [3]

[1] Faculty of Advanced Technologies and Chemistry, Military University of Technology, Warsaw, Poland; jarosz@wat.edu.pl (L.R.J.), anna.kurzych@wat.edu.pl (A.K.), zbigniew.krajewski@wat.edu.pl (Z.K.), michal.dudek@wat.edu.pl (M.D.)
[2] Elproma Electronics Ltd, Łomianki, Poland; j.kowalski@elpromaelectronics.com
[3] Institute of Geophysics, Polish Academy of Science, Warsaw, Poland; kt@igf.edu.pl
* Correspondence: jarosz@wat.edu.pl; Tel.: +48 261 839 014

Received: date; Accepted: date; Published: date

Abstract: The paper presents construction, laboratory tests as well as the first field application of a new fiber-optic rotational seismograph. The system based on fiber-optic gyroscope (FOG) with determined Angle Random Walk of the order of 10^{-8} rad/Sqrt(s) and a few rad/s maximum detectable amplitude of rotation in the frequency range from DC to 328.12 Hz. It has been designed for rotational seismology area of interest. This work also presents exemplary relevant measurements which were conducted using a set of two devices installed in the geophysical observatory in Książ, Poland.

Keywords: rotational seismograph, fiber optic sensor, rotational events, seismology, rotational seismology

1. Introduction

Paper deals with an innovative sensor suitable for rotational seismology which falls within rotational ground movements from earthquakes, explosions, and ambient vibrations [1]. These motions are interesting for several reasons and can also provide additional constraints on the seismic source [2, 3]. From above reasons, it is interesting to a wide range of geophysical disciplines, including broadband seismology, strong-motion seismology, earthquake engineering, seismic hazards, earthquake physics, seismic instrumentation, seismotectonics, geodesy, as well as to physicists connected with LIGO project. The practical aspect of the first three from the above disciplines might also have some effect on the rocking and torsion even accidental torsion of engineering construction as well as on the distortion of high or long structures [4].

In spite of growing popularity of the rotational seismology, there is still lack of appropriate rotational sensors for its field application also in the form of seismograph which contains rotational sensor, data acquisition system with precise sensor localization and precision time monitoring. One can distinguish several technologies of rotational sensors, starting from mechanical systems basing on pendulum seismometers [5] or geophones [6, 7] through MEMS gyro [8] up to ring laser [9]. Nevertheless, rotational sensors used in field application should meet some technical requirements forced by the rotational seismology which one can find in the paper [10]. Additionally, the issue of data relatability is also significant. To gather reliable data, one must apply at least two systems designed according to the same technology, like for instance in the well-known paper [11].

From the above reasons in this extended paper, regards manuscript showed on 7th International Symposium on Sensor Science (I3S2019) – Napoli [12], we describe the construction, laboratory test as well as results of field application of FOSREM® - the innovative Fiber-Optic Rotational Seismograph. During the field test conducted in the geophysical observatory in Książ, Poland, the torsion and tilt effects resulting from mining seismic quakes induced by copper mining operations have been recorded with high accuracy.

2. Construction and Laboratory Investigation of the Fiber-Optic Rotational Seismograph - FOSREM®

2.1. FOSREM® Construction

FOSREM® contains two main part: a rotational sensor and data center – a special WEB FOSREM (Telemetric Server) used for the data storage, monitoring the sensors' work, as well as for the remote control of their parameters. Because in the rotational seismology the rotational event exists as sudden changes, each sensor has been constructed by applying a minimum open-loop FOG configuration with a multi-integrated optical circuit (MIOC) where the Sagnac effect [13] produces a phase shift ($\Delta\phi$) between two counter-propagating light beams proportional to a measured rotation rate (Ω) [14]:

$$\Omega = S_o \Delta\phi = (\lambda c / 4\pi R L)\, \Delta\phi, \tag{1}$$

where S_0 - the optical constant of the system, λ - the wavelength of the used light source, c – the velocity of light in the vacuum, L - the length of fiber in the sensor loop, R - the sensor loop radius.

The main advantage of such solution is its practical insensitivity to linear motions and direct measurement of a rotational rate. Physically each sensor can be divided into two basic parts: optical and electronic. The optical part according to the schema in Figure 1 assures the Sagnac effect reversibility. To obtain FOSERM® sensitivity of the order of 10^{-8} rad/s/√Hz and simultaneously to minimalize the sensor dimension (up to 0.1075 m loop radius), length of the fiber sensor loop was optimized to 5000 m. The standard single mode fiber SMF-28e+ (*Corning, USA*) with attenuation 0.322 dB/km was wound as sensor loop using a special kind of winding named a double-quadrupole mode regards to minimalize thermal Shupe effect [15]. Used broadband source SLED (*Exalos, Switzerland*) with a bandwidth of 37.9 nm, a central wavelength of 1313.1 nm and optical power of 10 mW, lead to depolarization of beams propagating in the loop. This approach ensures the elimination of the polarization effect of interacting beams on the output signal [16].

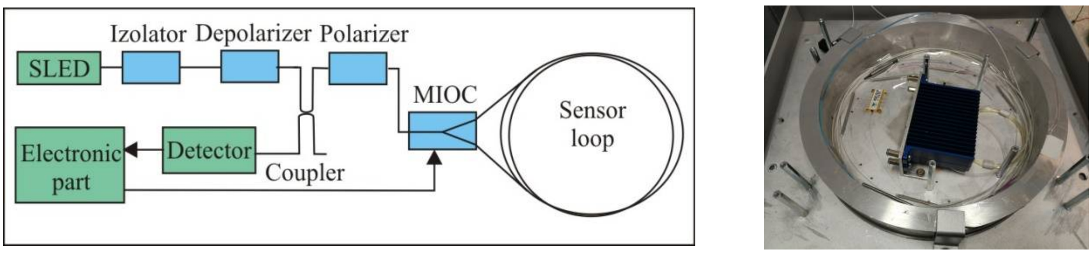

(**a**) (**b**)

Figure 1. The optical part of sensor according to a minimum gyro configuration: (**a**) block diagram, (**b**) technical realization for FOSREM-1.

Calculation of the detected rotation is based on the following equation [17]:

$$\Omega = S_o \arctan[S_e\, u(t)] = S_o \arctan[S_e\, (A_{1\omega}/A_{2\omega})], \tag{2}$$

where: $A_{1\omega}$, $A_{2\omega}$ is the first and second amplitude of the harmonic output signal $u(t)$, S_e - the electrical constant related with parameters of applied components. Above calculation is realized by the sensor's electronic part which realizes synchronous detection in a digital form with a special procedure of selecting and amplification of the first and second amplitude of harmonic output signal due to a large difference (4-5 orders of magnitude) of their amplitudes [17]. As one can see in Figure 2, the hardware of this part contains digital units with sophisticated software for system control and real-time data computation. The main element is the Z-turn Board (*XC7Z020-1CLG400C, MYIR*) based on the Xilinx Zynq-7000 all programmable SoC. It integrates a dual-core ARM Cortex-A9 based processing system and 28 nm Xilinx programmable logic in a single device. The Z-turn board

Peer-reviewed version available at *Sensors* **2019**, *19*, 2699; doi:10.3390/s19122699

allows communication by 10/100/1000 Ethernet and USB. All electronic modules (described below MAMP – amplifier, MFLT – filter, MSIN - MIOC signal generator, MLAS - SLED controller) are connected to IP core running on the FPGA using a hardware interface. The MAMP used for amplification of the detected signal is connected with a photodiode and contains a trans-impedance amplifier, low pass filter (FLT), PGA and 24-bits 1.5Msps analog-to-digital converter (ADC). The MFLT protects filtration of the first and second harmonic output signal and contains special digitally control band rejected filter (BRF), low pass filter, PGA and above described ADC. The analog signals in each channel are simultaneously sampled by each ADC connected to the FPGA chip. Applied analog pats define high accurate acquisition with almost 1Msps sampling and over 100 dB dynamic range. The MSIN protects suitable modulation analog signal for the MIOC, which 16-bit DAC connected to the FPGA chip works simultaneously with ADCs. Finally, the MLAS services the control and state signal of the light source SLED. Dedicated IP core collects raw data from ADCs transfers it to ARM Cortex-A9 processor which performs all computation including phase (continuously phase counting above 2π). It also realizes communication transfer to the communication unit or the Internet. The connection provides data transmission and power supply over a single STP cable within a distance of 100 m.

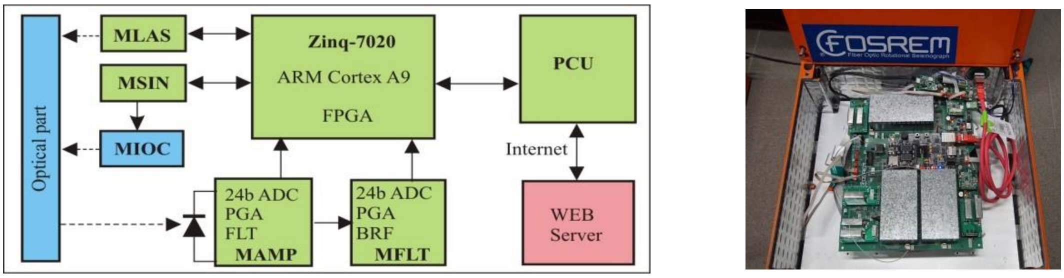

(**a**) (**b**)

Figure 2. The electronic part of sensor: (**a**) block diagram, (**b**) technical realization for FOSREM-1.

Finally, the obtained results are stored on a hard disc and transmitted to the telemetric server (WEB FOSREM) which additionally can be used for remote control all sensors (see Figure 3).

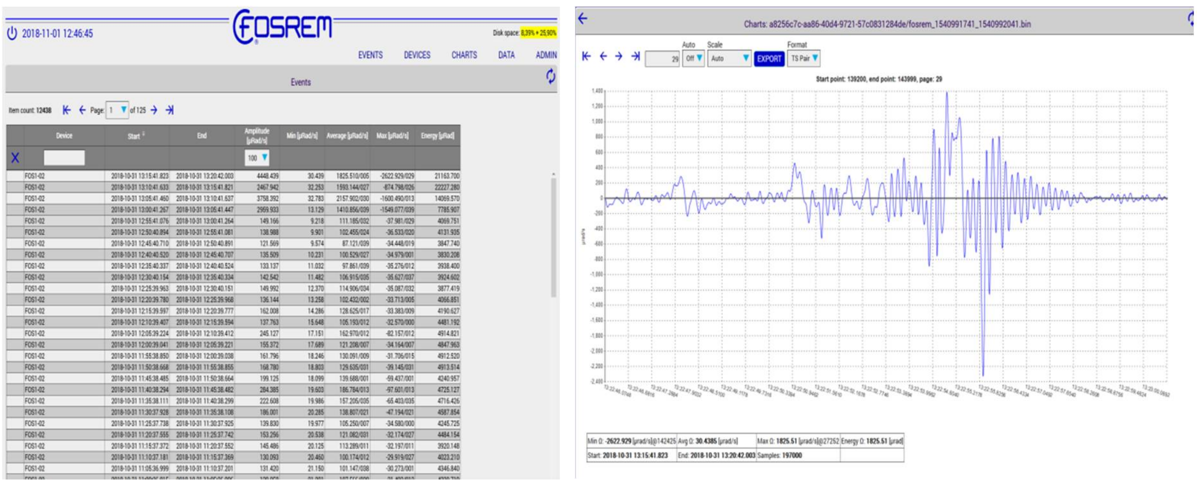

(**a**) (**b**)

Figure 3. Print Screen for WEB FOSREM: (**a**) screen with selected and stored by system events, (**b**) example of recorded seismic torsion event.

The remote control, possibility of the independent power supply and relatively small dimension of FOSREM (360x360x180 mm) and their weight ~10 kg makes it a fully mobile device.

Peer-reviewed version available at *Sensors* **2019**, *19*, 2699; doi:10.3390/s19122699

2.1. Results of Laboratory Investigation

The proper FOSREMs' work required in the first step their calibration by determination optical and electrical constants (S_o, S_e). This was made on the base of the Earth rotation measurement regards procedure in detail described in our previous paper [18]. Several experimental tests were carried out to confirm FOSREMs' parameters and reliability including experimental uncertainties calculation based on the registration of the rotational component of the Earth at different frequency bandpass [19], recording strong rotation motion with a new set-up using earthquake simulation [10] and other. As an example, in Figure 4(a) a thermal test in a climate chamber VCL 7010 (*Vötsch Industrietechnik, Germany*) at a temperature range 0 °C – 50 °C for FOSREM-2 is presented [19]. As one can see the recorded thermal instability of output signal is less than 0.06 %/°C including the cooling and heating cycle. Similarly we obtained good linearity for FOSREMs regarding detection rotation with high angular velocity up to radian per second (limitation of used measurement equipment) what is presented in Figure 4(b). The observed perturbation for angular velocity around 0.05, 0.10, 0.22 and 0.38 rad/s are connected with the resonant characteristic of the rotation table.

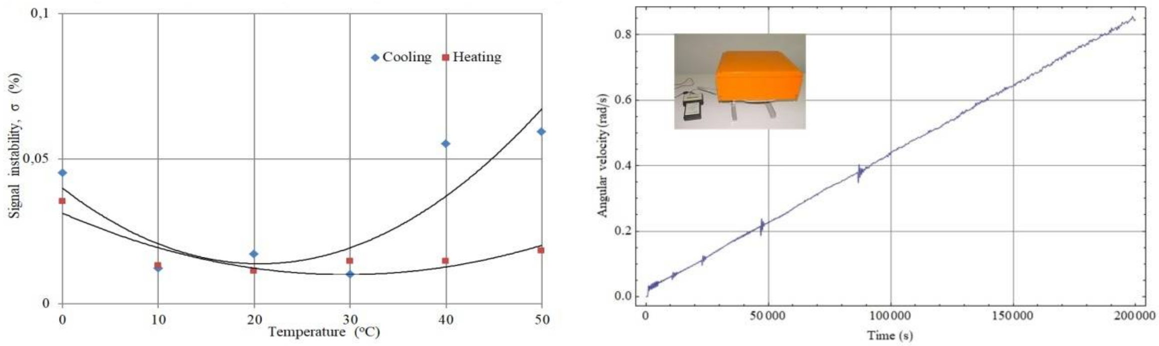

(**a**) (**b**)

Figure 4. Example of a laboratory test of FOSREM-2: (**a**) temperature stability for the cooling and heating cycle [19], (**b**) recording rotational speed with increasing angular velocity up to 0.9 rad/s.

Finally, regarding the investigation of the sensitivity of the system, as well as their drift, the Allan variance analysis (AV), have been performed [20, 21]. Figure 5 presents the result of these analyses for FOSREM-1 and -2. The data for AV were gathered at MUT in Warsaw for two positions of the FOSREMs: on the sturdy flat floor in basement of the laboratory and on an active optical table (*Thorlabs*). Moreover, the data were recorded in night hours in order to reduce urban noise. The plots presented on the Figure 5 points out that the appropriate method of the error estimating is significant, but environmental conditions are crucial and they can provide false results. The parameters of ARW (Angle Random Walk) and BI (Bias Instability) determined basing on data gathered when sensors were placed on the active optical table are more reliable. The plot on the Figure 5(a) is more disturbed and the values of ARW and BI based on this plot have higher value (Table 1). The disturbances on the Figure 5(b) are results of resonance characteristic of the applied table, nevertheless it indicates lower values of ARW and BI; ARW is equal to $8.66{\cdot}10^{-8}$ rad/√s and $2.45{\cdot}10^{-8}$ rad/√s whereas BI has a level of $1.13{\cdot}10^{-8}$ rad/s and $3.91{\cdot}10^{-9}$ rad/s for FOSREM-1 and -2, respectively.

Table 1. The parameters of ARW and BI for FOSREM-1, -2 determined basing on the data gathered in various positions of FOSREMs

	Sturdy flat floor		Active optical table	
	ARW [rad/√s]	BI [rad/s]	ARW [rad/√s]	BI [rad/s]
FOSREM-1	$1.33{\cdot}10^{-7}$	$1.81{\cdot}10^{-8}$	$8.66{\cdot}10^{-8}$	$1.13{\cdot}10^{-8}$
FOSREM-2	$5.26{\cdot}10^{-8}$	$8.08{\cdot}10^{-9}$	$2.45{\cdot}10^{-8}$	$3.91{\cdot}10^{-9}$

Preprints (www.preprints.org) | NOT PEER-REVIEWED | Posted: 6 May 2019 doi:10.20944/preprints201905.0061.v1

Peer-reviewed version available at Sensors 2019, 19, 2699; doi:10.3390/s19122699

The obtained value of ARW is in good correlation with the theoretical sensitivity of FOSREM mentioned in section 2.1. Taking into account the total losses of optical part (24.68 dB and 19.02 dB for FOSREM-1 and -2, respectively) the sensitivity equals $6.00 \cdot 10^{-8}$ rad/s/√Hz and $2.83 \cdot 10^{-8}$ rad/s/√Hz has been expected for FOSREM-1 and -2, respectively.

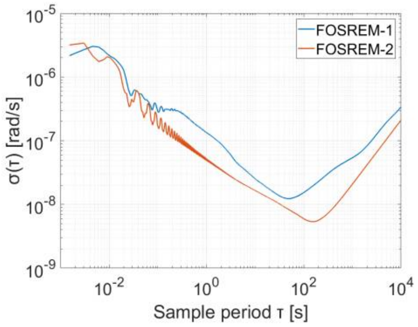

(**a**) (**b**)

Figure 5. The Allan variance analysis for FOSREM-1 and -2 determined basing on the data gathered in various positions of the FOSREMs: (**a**) sensors were placed on the sturdy flat floor in basement of the laboratory; (**b**) sensors were placed on the active optical table.

Because determined parameters fulfill all requirements described for rotational seismology [10], that can be concluded, so FOSREM seems to be appropriate for registration of rotational events associated with rotational seismology.

3. FOSREM® in the Field Application

The set of two FOSREMs (recognized by WEB FOSREM as FOSREM-1 and FOSREM-2) have been mounted in the geophysical observatory of the Polish Academy of Science in Książ, Poland which is located in the area of mining activity (position ϕ=50°50'31"N, λ=16°17'29"E). The seismometers have been installed on special pedestal mounted for seismological measurement located at a depth of about 49 m below the main castle courtyard next to each other (Figure 6).

(**a**) (**b**)

Figure 6. FOSREMs' field application: (**a**) Książ castle with view on the underground tunnel locates at the level of 49 m below the surface of the castle, (**b**) mounted devices in the geophysical observatory.

The obtained data [stored at WEB FOSREM as events – see example in Figure 3(b)] were analyzed in a specially designed Matlab script which allows to read the data from both FOSREMs simultaneously and to calculate the Pearson's correlation coefficient (P_C) between the signals from FOSREMs according to the following formula [22]:

$$P_c = cov(x, y)/(\sigma_x \sigma_y), \quad (3)$$

Preprints (www.preprints.org) | NOT PEER-REVIEWED | Posted: 6 May 2019 doi:10.20944/preprints201905.0061.v1

Peer-reviewed version available at *Sensors* **2019**, *19*, 2699; doi:10.3390/s19122699

where: *cov*(x,y) – the covariance between variables *x* and *y*, σ_l – the standard deviation in the population *l*.

Figure 7 presents the exemplary data of the recorded torsion and tilt by two installed devices. The average value of the P_C between presented signals is of the order of 0.98 and 0.57 which indicates very good compatibility of the waveforms, especially for torsion event. Every figure also shows information about the absolute value of the maximal amplitude of the signal (|F-1 max|, |F-2 max|), as well as an E_F - energy coefficient ($E_{|F-1|}$, $E_{|F-2|}$) for FOSREM-1 and FOSREM-2, respectively.

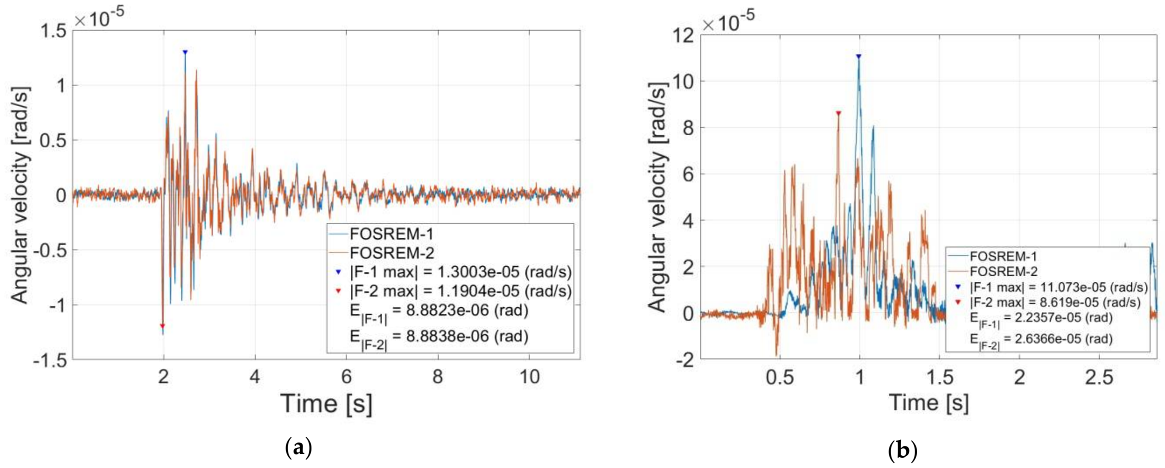

Figure **7.** The example of data recorded by the FOSREMs in the geophysical observatory in Książ, Poland: (**a**) torsion event on the 1st December 2017, at 12:19 UTC, (**b**) tilt event on the 13th December 2017, at 11:15 UTC.

In Table 1, we present a collection of recorded same torsion and tilt events in period 29/08/2017 – 3/02/2018. There are information about recorded by FOSREMs maximal signal amplitude, energy

Table 1. Data recorded by the FOSREMs in the geophysical observatory in Książ, Poland in period 29/08/2017 – 3/02/2018

Device	Recorded torsion event					Recorded tilt event				
	Date	Time	Max. amplitude [rad/s]	E_F [rad]	P_c	Date	Time	Max. amplitude [rad/s]	E_F [rad]	P_c
FOSREM-1	29/08/17	11:02:34	$2.68\cdot10^{-5}$	$1.31\cdot10^{-5}$	0.99	08/12/17	13:01:41	$9.61\cdot10^{-5}$	$2.19\cdot10^{-5}$	0.71
FOSREM-2			$3.25\cdot10^{-5}$	$1.91\cdot10^{-5}$				$9.31\cdot10^{-5}$	$2.20\cdot10^{-5}$	
FOSREM-1	29/08/17	11:08:12	$1.23\cdot10^{-5}$	$9.00\cdot10^{-6}$	0.98	13/12/17	11:15:27	$1.11\cdot10^{-4}$	$2.34\cdot10^{-5}$	0.57
FOSREM-2			$1.21\cdot10^{-5}$	$9.12\cdot10^{-6}$				$8.62\cdot10^{-5}$	$2.64\cdot10^{-5}$	
FOSREM-1	01/12/17	12:19:10	$1.30\cdot10^{-5}$	$8.88\cdot10^{-6}$	0.98	11/01/18	11:27:05	$7.97\cdot10^{-6}$	$1.89\cdot10^{-6}$	0.59
FOSREM-2			$1.19\cdot10^{-5}$	$8.88\cdot10^{-6}$				$8.46\cdot10^{-6}$	$1.61\cdot10^{-6}$	
FOSREM-1	13/12/17	18:25:43	$3.03\cdot10^{-6}$	$2.22\cdot10^{-6}$	0.93	18/01/18	9:44:34	$5.21\cdot10^{-5}$	$1.52\cdot10^{-5}$	0.59
FOSREM-2			$3.26\cdot10^{-6}$	$2.56\cdot10^{-6}$				$5.47\cdot10^{-5}$	$1.23\cdot10^{-5}$	
FOSREM-1	13/12/17	18:25:58	$1.78\cdot10^{-6}$	$1.18\cdot10^{-6}$	0.92	25/01/18	11:55:33	$9.35\cdot10^{-4}$	$1.03\cdot10^{-4}$	0.67
FOSREM-2			$2.08\cdot10^{-6}$	$1.52\cdot10^{-6}$				$8.76\cdot10^{-4}$	$1.17\cdot10^{-4}$	
FOSREM-1	14/12/17	08:06:24	$6.04\cdot10^{-6}$	$4.26\cdot10^{-6}$	0.97	26/01/18	11:11:18	$2.34\cdot10^{-4}$	$3.77\cdot10^{-5}$	0.60
FOSREM-2			$6.13\cdot10^{-6}$	$4.80\cdot10^{-6}$				$2.21\cdot10^{-4}$	$3.78\cdot10^{-5}$	
FOSREM-1	08/01/18	08:09:02	$3.88\cdot10^{-6}$	$4.43\cdot10^{-6}$	0.95	26/01/18	11:11:43	$4.99\cdot10^{-4}$	$4.92\cdot10^{-5}$	0.57
FOSREM-2			$3.44\cdot10^{-6}$	$4.66\cdot10^{-6}$				$6.61\cdot10^{-4}$	$5.82\cdot10^{-5}$	
FOSREM-1	08/01/18	08:09:57	$1.18\cdot10^{-5}$	$9.31\cdot10^{-6}$	0.98	26/01/18	11:11:58	$4.98\cdot10^{-4}$	$5.76\cdot10^{-5}$	0.73
FOSREM-2			$1.29\cdot10^{-5}$	$9.56\cdot10^{-6}$				$4.78\cdot10^{-4}$	$4.95\cdot10^{-5}$	
FOSREM-1	26/01/18	11:14:23	$1.42\cdot10^{-5}$	$1.22\cdot10^{-5}$	0.97	03/02/18	10:14:21	$2.40\cdot10^{-4}$	$4.25\cdot10^{-5}$	0.61
FOSREM-2			$1.40\cdot10^{-5}$	$1.21\cdot10^{-5}$				$2.85\cdot10^{-4}$	$5.64\cdot10^{-5}$	
Average value of P_c for torsion event				**0.96 ± 0.03**		**Average value of P_c for tilt event**			**0.63 ± 0.6**	

coefficient (E_F) calculated numerically using a method of rectangles of the Riemann integral as well as the correlation coefficient (P_C) between FOSREM-1 and FOSREM-2. The energy coefficient of tilt can be physically directly indicated with a value of an angle of a rock's crump.

One can see that torsion recording is characterized by the higher value of the P_C (0.96 ± 0.03) between the FOSREMs than for tilt recordings (0.63 ± 0.03). We concluded that high correlation of torsion events recorded by FOSREM-1 and FOSREM-2 indicated good compatibility of the FOSREMs' signals could be treated as proof of their usefulness for recording rotational events. On the other hand, a much smaller correlation obtained for recorded tilt is thought-provoking. It is a little information in the literature about tilt recording, so our results are probably one of the first in this matter. The relative small average value of P_C for them (0.63 ± 0.03) can be connected with the method of FOSREMs mounted at the seismological pedestal. Instead of sensor putting there should be stiff mounted to the base even if their relatively high weight (about 10 kg) because the tilt is in the range of ten milliradians. As one can see from data presented in Table 1, the value of the maximal recorded amplitude ($9.35 \cdot 10^{-4}$ rad/s), as well as energy coefficient ($1.17 \cdot 10^{-4}$ rad) for tilt events, is much higher than for recorded torsion events ($3.25 \cdot 10^{-5}$ rad/s; $1.91 \cdot 10^{-5}$ rad). The nature of the tilt phenomenon which is more rapid due to its source of generation, for example, caving, probably needs better sensor protection against itself moving.

5. Conclusions

The FOSREM® - Fiber-Optic Rotational Seismograph, presented in this paper seems to be a suitable instrument for rotational seismology. It used the mobile fiber-optic rotational seismometers enabling to detect rotational movements in wide amplitude (from $3\text{-}6 \cdot 10^{-8}$ rad/s up to a few rad/s) as well as suitable frequency range (from DC up to 328.12 Hz). Because the FOSREM® is fully remote controlled by the internet, it is suited for autonomous work in a very long period. Thus it is useful for a systematic seismological investigation at any place.

The collected data in the geophysical observatory in Książ, Poland are resulting from mining seismic quakes induced by copper ore mining operations. Their recording by a set of two FOSREMs shows a very high correlation coefficient between the applied sensors regards torsion events which confirm the records' reliability. The data connected with tilt events are not so good correlated, but probably it is caused by wrong sensor connection with seismological pedestal. However, the collected data indicated the rapid nature of tilt phenomenon which is reflected in the higher value of recorded signal amplitude than in the case of torsion recordings. In authors' knowledge, the presented in this paper recordings of tilt effects caused by crumps at local mines are one of the carried out research in the world. FOSREM® gives great opportunities for spreading knowledge about seismic rotational events, as well as torsional effects existing in any engineering constructions. On the above, in authors opinion the presented FOSREM® is appreciated for realizing the growing interest in rotational seismology by providing significant data.

Author Contributions**:** conceptualization, L.R.J.; methodology, L.R.J. and A.K.; software, J.K.K. and M.D.; resources, J.K.K.; validation, A.K. and Z.K.; investigation, K.P.T.; writing—draft, review and editing, A.K. and L.R.J.

Acknowledgments: This work was financially supported by the Ministry of the National Defence Republic of Poland - project GBMON/13-995/2018/WAT, program POIR.04.02.00-14-A003/16 "EPOS – System Obserwacji Płyty Europejskiej" as well as the National Science Centre, Poland - project 2016/23/N/ST10/02508.

Conflicts of Interest: The authors declare no conflict of interest.

References

1. Lee, W.H.K.; Celebi, M.; Todorovska, M.I.; Igel, H. Introduction to the special issue on rotational seismology and engineering applications. *Bull. Seismol. Soc. Am.*, **2009**, *99(2B)*, 945-957.
2. Spudich, P.; Fletcher, J.B. Observation and prediction of dynamic ground strains, tilts, and torsions caused by the M_w 6.0 2004 Parkfield, California earthquake and aftershocks, derived from USPAR Array observations. *Bull. Seismol. Soc. Am.*, **2008**, *98*, 1898–1914.

3. Takeo, M.; Ito, H.M. What can be learned from rotational motions excited by earthquakes? *Geophys. J. Int.*, **1997**, *129*, 319-329.
4. Trifunac, M.D. A note on rotational components of earthquake motions on ground surface for incident body waves. *Soil Dyn. and Earthquake Eng*., **1982**, *1*, 11-19.
5. Kurzych, A.; Teisseyre, K.P.; Krajewski, Z; Jaroszewicz L.R. Rotational components of the seismic fields caused by local events. In *Earthquake Engineering - From Engineering Seismology to Optimal Seismic Design of Engineering Structures*, 1st ed.; Moustafa, A. Ed.; Intech: Rijeka, Croatia, 2015: pp. 163 - 188.
6. Brokešová, J.; Málek, J.; Štrunc, J. Rotational seismic sensor system, seismic measuring set containing that system, and seismic survey method. Patent no. CZ 301217 B6, 2009.
7. Brokešová, J.; Málek, J. Six-degree-of-freedom near-source seismic motions I: rotation-to-translation relations and synthetic examples. *J. Seismol.*, **2015**, *19*, 491-509.
8. D'Alessandro, A.; D'Anna, G. Suitability of low-cost three-axis MEMS accelerometers in strong-motion seismology: Tests on the LIS331DLH (iPhone) accelerometer. *Bull. Seismol. Soc. Am*., **2013**, *103*, 2906-2913.
9. Schreiber, K.U.; Hautmann, J.N.; Velikoseltsev, A.; Wassermann, J.; Igel, H. et al. Ring laser measurements of ground rotations for seismology. *Bull. Seismol. Soc. Am*., **2009**, *99(2B)*, 1190-1198.
10. Jaroszewicz, L.R.; Kurzych, A.; Krajewski, Z.; Marc, P.; Kowalski, J.K; et al. Review of the usefulness of various rotational seismometers with laboratory results of fibre-optic ones tested for engineering applications. *Sensors*, **2016**, *16(12)*, 2161.
11. Abbott, B.P;. Abbott, R.; Abbott, T.D.; Abernathy, M.R.; Acernese, F.; et al. Observation of gravitational waves from a binary black hole merger. *Phys. Rev. Lett*., **2016**, *116*, 061102.
12. Jaroszewicz, L.R.; Kurzych, A.; Krajewski, Z.; Kowalski, J.K.; Kowalski, H.A.; Teisseyre, K.P. Innovative fiber-optic rotational seismograph. Proceedings of the 7th International Symposium on Sensor Science (I3S 2019), Napoli, Italy, 9-11 May 2019, MDPI, https://www.mdpi.com/journal/proceedings.
13. Sagnac, G. L'ether lumineux demontre par l'effet du vent relatif d'Etherdanus un interferometre en rotation uniforme. *C. R. l'Acad. Sci*. **1913**, *95*, 708-710.
14. LeFevre, H.C. *The Fiber Optic Gyroscope*, 2nd ed., Ed. Norwood: Artech House, USA, **2014**, 38-53.
15. Dai, X.; Zhao, X.; Cai, B.; Yang, G.; Zhou, K.; Liu, C. Quantitative analysis of the Shupe reduction in a fiber-optic Sagnac interferometer. *Opt. Eng*., **2002**, *41(6)*, 1155–1156.
16. Ezekiel, S.; Davis, J.L.; Hellwarth, R.W. Observation of intensity-induced nonreciprocity in a fiber-optic gyroscope. *Optics Lett*., **1982**, *7*, 457-459.
17. Kurzych, A.; Jaroszewicz, L.R.; Krajewski, Z.; Sakowicz, B.; Kowalski, J.K.; Marć P. Fibre-optic Sagnac interferometer in a FOG minimum configuration as instrumental challenge for rotational seismology. *J. Lightwave Techn*., **2018**, *36*, 879-884.
18. Jaroszewicz, L.R.; Krajewski, Z.; Kowalski, H.; Mazur, G.; Zinówko, P.; Kowalski, J. AFORS - Autonomous Fibre-Optic Rotational Seismograph: design and application. *Acta Geophys*., **2011,** *59(3)*, 578-596.
19. Kurzych, A.; Kowalski, J.K;. Sakowicz, B.; Krajewski, Z.; Jaroszewicz, L.R. The laboratory investigation of the innovative sensor for torsional effects in engineering structures' monitoring. *Opto-Electron. Rev*., **2016**, *24*, 134-143.
20. IEEE Standard specification format guide and test procedure for single-axis interferometric Fiber Optic Gyros. New York: IEEE-SA Standards Board, **1997**.
21. Allan variance: noise analysis for gyroscopes. *Freescale Semiconductor Application Note AN5087*, 0,2/2015, **2015**.
22. Hall, G. Pearson's correlation coefficient. Available online: http://www.hep.ph.ic. ac.uk/~hallg/UG_2015/ Pearsons.pdf (access on 13 March 2018)